AGU PUBLICATIONS

Journal of Advances in Modeling Earth Systems

RESEARCH ARTICLE
10.1002/2016MS000903

Resolution dependence of extreme precipitation and deep convection over the Gulf Stream

Sebastian Scher[1,2], Reindert J. Haarsma[1], Hylke de Vries[1], Sybren S. Drijfhout[1,2,3], and Aarnout J. van Delden[2]

[1]Weather and climate models, Royal Netherlands Meteorological Institute (KNMI), De Bilt, Netherlands, [2]Institute for Marine and Atmospheric Research (IMAU), Utrecht University, Utrecht, Netherlands, [3]Ocean and Earth Science, National Oceanography Centre Southampton, University of Southampton, UK

Key Points:
- There is an increase of extreme wintertime precipitation and deep convection with increasing model resolution
- Increase in resolution leads to better agreement with observations

Supporting Information:
- Supporting Information S1

Correspondence to:
R. Haarsma,
haarsma@knmi.nl

Citation:
Scher, S., R. J. Haarsma, H. de Vries, S. S. Drijfhout, and A. J. van Delden (2017), Resolution dependence of extreme precipitation and deep convection over the Gulf Stream, *J. Adv. Model. Earth Syst.*, *9*, doi:10.1002/2016MS000903.

Received 23 DEC 2016
Accepted 29 APR 2017
Accepted article online 8 MAY 2017

Abstract Modeled wintertime precipitation over the Atlantic Gulf Stream region is shown to be sensitive to the horizontal resolution of the driving Global Circulation Model (GCM). By contrasting simulations with the EC-Earth GCM over a range of horizontal resolutions (T159, T319, T799), it is shown that especially the precipitation extremes become more populated if resolution is higher. Higher resolution also appears to strengthen the communication from the sea surface toward the troposphere. With increasing resolution, deep convection over the Gulf Stream region, diagnosed via wind-convergence and vertical motion, occurs more frequently and the former is in better agreement with observations. Likewise the frequency increase of the precipitation extremes over the region for increasing resolution makes them agree better with observations, despite large natural variability and discrepancies between different observational sources.

1. Introduction

Global Climate Models (GCMs) are widely used to describe Earth's present climate. They are our main working horse to get to understand the sensitivity of our climate to all kinds of processes, interactions, and feedbacks. We even run them forward in time under different forcing scenarios to get projections of future climate.

A typical state of the art GCM is run at a spatial resolution of ~100 km. At this horizontal resolution, it is generally able to capture the current climate reasonably well in terms of temperature, pressure, and vorticity, especially at the larger spatial scales. However, it performs much less in replicating observed precipitation [*Flato et al*., 2013]. GCMs typically show too many precipitation events that in addition have too low intensity [*Stephens et al*., 2010]. Increasing horizontal model resolution is one of the options to improve on this, as precipitation is to large extent parameterized. Moreover, as climate projections start to be done with GCMs with resolution higher than 100 km [e.g., *Kitoh and Endo*, 2016], it is of importance to know the impact that increasing resolution has on modeled precipitation.

The present paper explores the effect of increasing horizontal resolution on the structure and intensity of the precipitation over a specific region of the North Atlantic, the Gulf Stream. This region is societally relevant and scientifically interesting from several perspectives. We mention the two most important motivations for this study. First, due to the high temperature contrasts in the region, especially in winter, a possibly important role is played by (deep) convection. As convective precipitation is largely parametrized in the GCMs, these regions are likely the first to be impacted (and hopefully benefit) from the increased resolution. Second, the Gulf Stream lies at the upstream start of the Atlantic storm track. It is the genesis region for midlatitude storms that are fueled by baroclinic instability. This implies that precipitation changes are carried downstream rapidly influencing the entire North Atlantic possibly as far as Europe where storms often reach full maturity. Precipitation in the midlatitudes is tightly coupled to the position and the intensity of storm tracks, and a better represented storm track seems to be key to also improve precipitation patterns. And indeed this is what has been reported before. *Zappa et al*. [2013] and *Colle et al*. [2013] showed that GCMs with high spatial resolution generally have a better represented North Atlantic storm track, and *van Haren et al*. [2015] showed that the increase of horizontal resolution leads to improved precipitation statistics over Europe. *van der Wiel et al*. [2016] showed that an increase in horizontal resolution leads to better

representation of precipitation extremes above the land part of the United States. [*Feng et al*., 2017] showed that increased resolution results in a better precipitation climatology over the Gulf stream region. However, the impact on extreme precipitation over that region is still an open question.

As discussed above, the Gulf Stream is an interesting region to study precipitation, because of the possibility of large-scale (deep) convection. These regions are probably the only in winter-time outside the tropics where deep convection occurs. Observing rainfall is relatively straightforward with nowadays technology, although the localized nature of precipitation makes records notoriously noisy. However, collecting observations of (deep) convection and, more generally of the vertical motion field is very hard, especially over sea. The latter, however, is important to obtain insight in the underlying dynamics.

Linking intense vertical motion and extreme precipitation is not new of course. An overview of recent literature is now given. *Yang et al*. [2014] showed that resolution dependence of extreme precipitation is mainly caused by changes in dynamics related to vertical velocity. *Czaja and Blunt* [2011] showed with theoretical considerations and reanalysis data that in midlatitudes above oceanic boundary currents convection through the whole troposphere can occur, allowing the Sea Surface Temperatures (SSTs) to be "communicated" through the entire troposphere. Therefore, capturing of these convective events by models might be crucial for precipitation performance. Furthermore, it is known that sharp SST-fronts occurring together with boundary currents in the ocean have a significant impact on storm tracks and precipitation [*Small et al*., 2014; *Minobe et al*., 2008]. Since an atmospheric model with low spatial resolution "sees" only a very crude representation of these SST-fronts and eddies, increasing model resolution might also change precipitation and convection indirectly through better resolved ocean-atmosphere interaction. *Ma et al*. [2015] confirmed this by showing that small-scale SST variability in the Gulf Stream region affects the atmospheric circulation.

The two central questions of this paper are first how wintertime (DJF) extreme precipitation and deep convection statistics over the Gulf Stream change as a result of increasing resolution, and second whether these changes lead to better correspondence with the observations.

2. Data and Methods

Three runs with different horizontal resolution were made with the atmosphere-only part of the GCM EC-Earth. The use of an atmosphere-only model for investigating precipitation extremes is justified because of those occur at short (daily) time scales for which the ocean heat capacity can be considered infinite. EC-Earth is a state-of-the art climate model, based on the Integrated Forecast System (IFS) from ECMWF [see *Hazeleger et al*., 2012]. Each of the three runs consists of six ensemble members, where each member is run for 5 years (2002–2006), thus comprising 30 years for each resolution. The runs differ only in resolution of the model, with all other settings kept the same. The low-resolution model has a spectral resolution of T159L62, corresponding to approximately 1.1° or 125 km with 62 vertical layers. The intermediate resolution model has a spectral resolution of T319L92, corresponding to 0.56° or 62 km with 92 vertical layers, and the high-resolution model has a spectral resolution of T799L91, corresponding to approximately 0.25° or 28 km with 91 vertical layers. Due to storage limitations, only five pressure levels of saved data are available. For a more detailed description of the runs, see *Haarsma et al*. [2013]. We shall from now on refer to the low-resolution run as EC-Earth T159, to the intermediate resolution run as EC-Earth T319, and to the high-resolution run as EC-Earth T799. We will focus our analysis on the low and the high-resolution model, and use the intermediate resolution model as support. The external forcing consists of prescribed greenhouse gas concentrations and prescribed fields of sea surface temperatures (SSTs) and sea ice concentrations. As SST and sea ice data version 2 of the NOAA 1/4° daily Optimum Interpolation Sea Surface Temperature data set [*Reynolds et al*., 2007] was used. For validation, the model data sets are compared to precipitation and wind observations and the ERA-interim reanalysis.

ERA-Interim [*Dee et al*., 2011] is a reanalysis data set from 1979 to present, based on IFS with a spectral resolution of T255 (∼0.75°) and time resolution of 6 h. *Bosilovich et al*. [2011] noted that reanalysis are not continuous data sets, as the type and amount of observations changes over time, which can even cause unphysical jumps of variables. Nevertheless, ERA-Interim provides a dynamically consistent data set for our study. For monthly mean precipitation, the monthly version or the GPCPv2.2 precipitation data set [*Adler et al*., 2003] was used for the period 1985–2014. GPCP is a merged analysis of low-orbit satellite microwave

data, geostationary satellite infrared data, and rain gauges (the latter play only an indirect role as calibration in our study area). GPCPv2.2 has a resolution of 2.5 × 2.5°. For daily analyses, the GPCP 1dd [*Huffman et al*., 2001], CMORPH0.5 [*Joyce et al*., 2004], and TRMM version 7.0 [*Huffman et al*., 2010] data sets were used. Both CMORPH0.5 and TRMM have a spatial resolution of 0.25 × 0.25°.

For surface wind observations, the satellite observations from the Cross-Calibrated Multi-Platform Ocean Surface Wind Vector L3.0 First-Look Analyses (CCMP) for the period 1988–2011 were used [*Atlas et al*., 2011].

2.1. Comparing Data at Different Resolutions

Precipitation is not a continuous field. Therefore model-grid points at different spatial resolutions cannot directly be compared to each other. To deal with this problem, all fields were mapped to the T159 grid using second-order conservative remapping [*Jones*, 1999].

3. Results

3.1. Mean Precipitation

First, we assess the impact of horizontal resolution on the mean precipitation in EC-Earth. We will discuss here only the difference between T159 and T799. The impact of the intermediate T319 is less but qualitatively similar. Figure 1 shows the average DJF precipitation for all 30 years of the EC-Earth T159 simulation (top-left) as well as the difference T799-T159 (top-right). The increase of horizontal resolution leads to an increase in the mean precipitation south of the SST front. This is different from *Feng et al*. [2017], who found for the Athena simulations [*Jung et al*., 2012] the largest increase around 50W over the SST front. Although both EC-Earth and the Athena simulations are based on the ECMWF model, the model versions differ. This might explain the differences. Another cause could be that the resolution in Athena (T1279) is higher than EC-Earth (T799) and that the impact of the SST front is more prominent at higher resolutions. Decomposing the precipitation into stratiform (bottom right) and convective (bottom left) reveals that the change in stratiform precipitation is similar to *Feng et al*. [2017], although slightly more displaced to the south, but that the increase in convective precipitation at 50°W over the SST front is much less and more pronounced southward at 70°W and 30°S. Note, however, that the division between stratiform and convective precipitation is very much dependent on the details of the parameterization of convection.

The precipitation changes might partially be induced by changes in the large-scale features of the atmospheric circulation (temperature, wind, and humidity). An important characteristic of the atmospheric circulation is the location of the jet stream. It determines the storm track and systematic northward or southward shifts will likely result in an associated precipitation response. Jet-stream position is defined here as the latitude (northward of 27°N) where the 6 hourly wind speed at 300 hPa reaches its maximum. Figure 2 shows the mean wintertime location and the 25–75% range of the jet-stream position in the low and high-resolution version of EC-Earth (left plot) and in ERA-Interim (right plot). Over the Gulf Stream, both resolutions are virtually indistinguishable and give a realistic representation of the observed situation. Further downstream (eastern part North Atlantic and over Europe) the differences are somewhat larger, with T159 underestimating the spread compared to ERA-Interim. The overall similarity of the patterns indicates no systematic differences in the planetary wave structure, especially over the target area. However, the jet-stream location is only one aspect of the large-scale flow. Other parameters such as 850 hPa mean temperature, zonal wind, and specific humidity show that the story is more complex. For example, there is a significant increase (up to 0.5 K) in mean temperature at 850 hPa in the study region (supporting information Figure S1). Consistent with this increase, specific humidity also increases over almost the entire region (supporting information Figure S2), providing a natural tendency to enhance precipitation even if circulation were to remain constant. At the same time, the zonal wind at 850 hPa reduces (supporting information Figure S3). In conclusion, although the jet stream location remains unchanged, the increases seen in particular in temperature and humidity might also contribute to the precipitation changes. Differences in the circulation response between the Athena simulations and EC-Earth T799 might therefore be another source for the different mean precipitation response.

3.2. Extreme Precipitation

The impact of model resolution becomes more prominent for extreme precipitation events. Figure 3 shows the fraction of wintertime days with more than 30 mm precipitation for EC-Earth T159 and T799, analyzed

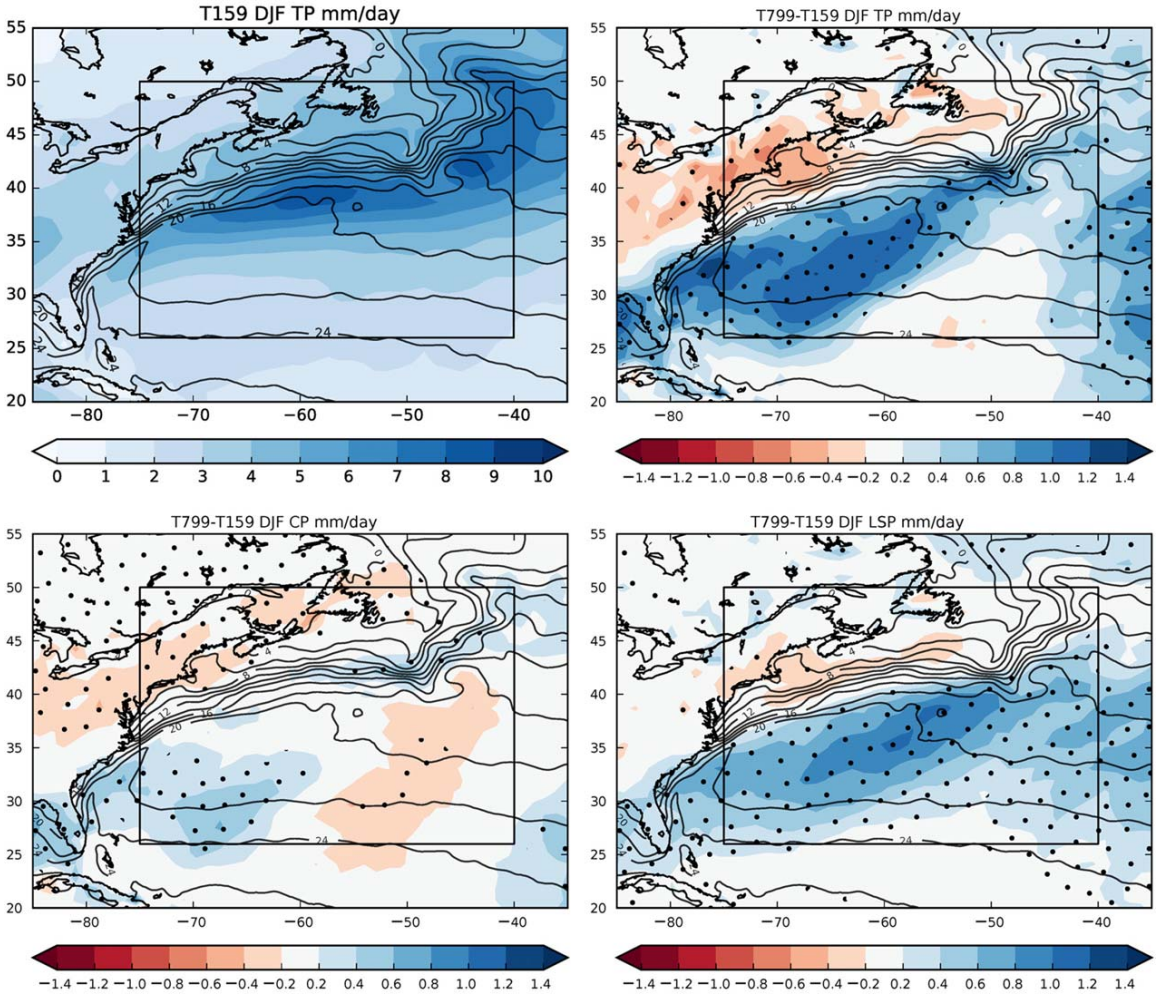

Figure 1. (top left) Wintertime rainfall for the present climate for EC-Earth T159, (top right) difference between T799 and T159, (bottom left) difference in Convective Precipitation (CP) between T799 and T159, and (bottom right) difference in Large Scale Precipitation (LSP) between T799 and T159. The black rectangle denotes the study region. Stippling indicates differences significant with $p = 0.05$.

for each grid point. There is a clear increase in frequency with higher-resolution, especially in the vicinity of the SST front.

A more detailed picture can be gained from Figure 4, which shows histograms of daily precipitation over the study area. The 5–95% confidence ranges were computed with bootstrapping daily events. All model

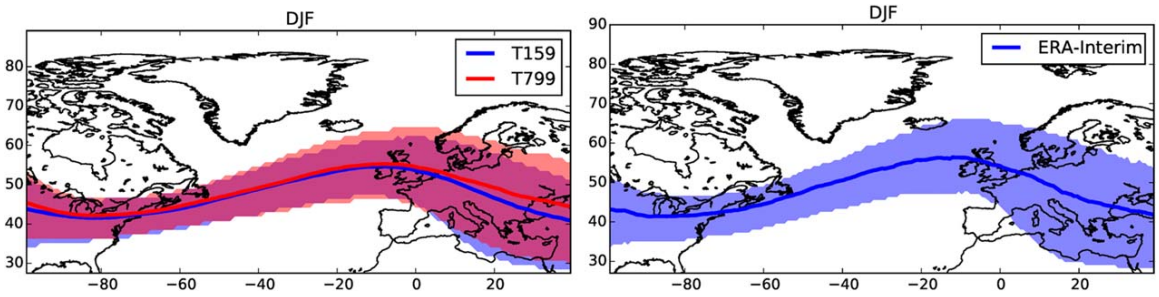

Figure 2. Location of the wintertime jet stream at 300 hPa. Line denotes the mean and shading the 25–75% range of the position.

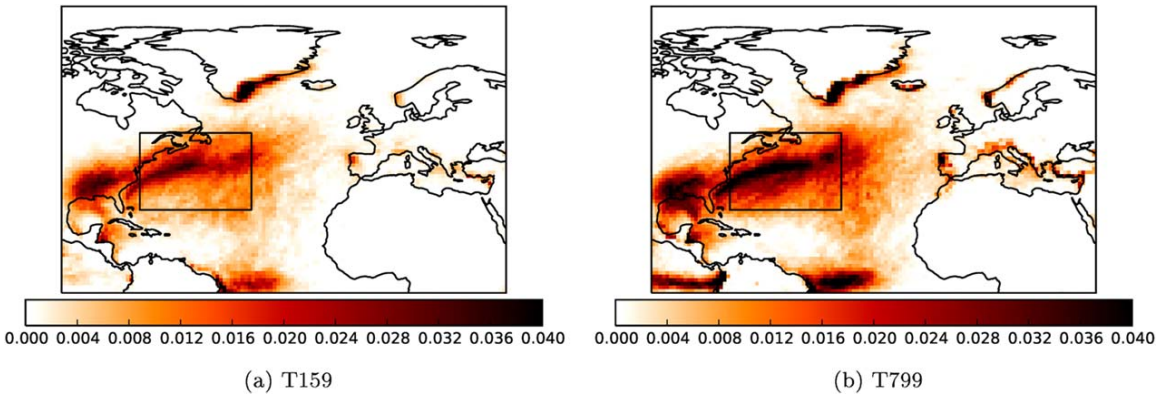

Figure 3. Fraction of wintertime days with precipitation exceeding 30 mm/d, analyzed for each grid point, for (a) the low-resolution and (b) the high-resolution version of EC-Earth.

resolutions and ERA-interim have significantly fewer dry days, and more days with low rainfall amounts ($<$5 mm/d) than observations. This result is qualitatively insensitive to the low-rainfall criterion for values between 4 and 8 mm/d. This discrepancy may in fact be caused by a deficiency in the observations, which use infrared satellite data, known to underestimate low precipitation (see *Joyce et al*. [2004] for CMORPH and *Adler et al*. [2003] for GPCP). On the other hand, models are also known to simulate too many drizzle days, which are part of the days with rainfall below 4 mm/d. [e.g., *Stephens et al*., 2010]. As it is for these reasons hard to draw solid conclusions from this part of the rainfall distribution, we turn attention to the right tail.

Here the effect of resolution increase is more promising. Above 30 mm/d GPCP and TRMM give higher values than the model at all resolutions and the model always gives higher values with increasing resolution. CMORPH, however, gives much lower estimates than GPCP and TRMM. For the bins of 29 and 33 mm/d CMORPH estimates are below all model values, and between bins 37 and 41 mm/d CMORPH estimates are below the T799 values. Only for values of 49 mm/d CMORPH estimates exceeds all model values. We note that *Feng et al*. [2017] concluded the beneficial effect of model resolution by comparing to TRMM only. We assume there is no reason for preferring either of the observational products. We consider the spread between the observations as an estimation of the observational uncertainty around their mean. With the increase of resolution *all* bins up to 50mm/d get systematically closer to the mean of the three observational estimates. Thus the higher-resolution promotes more extreme precipitation to occur in the region, and these correspond better to the observed record. These results are obtained using observations from the period 2002–2006 only. They are however qualitatively reproduced if we consider the extended observational period (supporting information Figure S4).

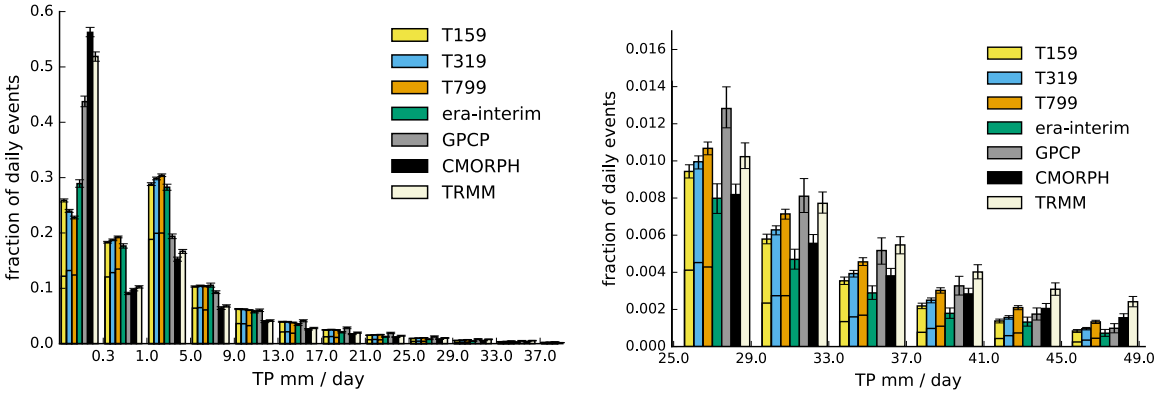

Figure 4. Distribution of wintertime daily Total Precipitation (TP) events in the study area for EC-Earth T159/T319/T799, ERA-Interim, GPCP, CMORPH, and TRMM 1dd data for 2002–2006. The x-ticks indicate the borders of the used bins. Both plots show the same data but with different scales. The error bars indicate the 5–95% confidence interval estimated with bootstrapping daily events. The height of the lower part of each bar with respect to the total height of the bar represents the fraction of convective precipitation.

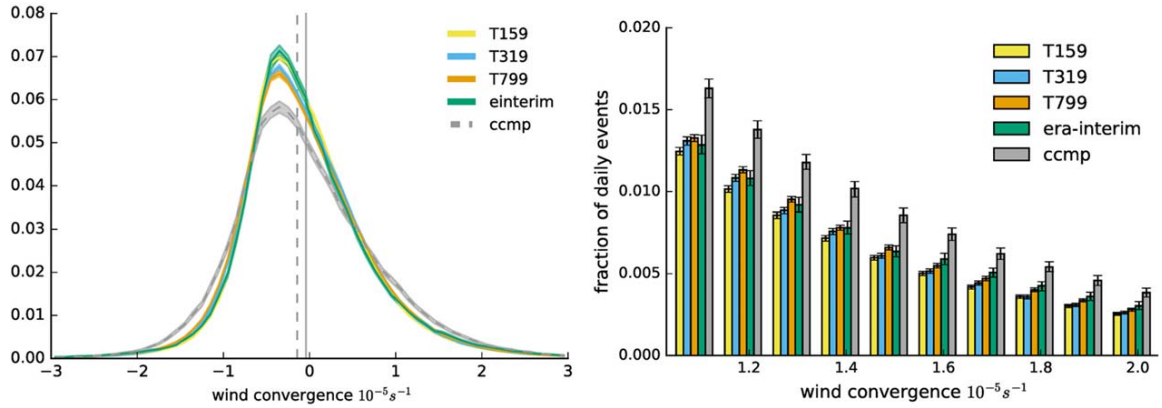

Figure 5. As Figure 4, but for wintertime daily mean horizontal wind convergence. For readability, the left plot is plotted with lines instead of bars. The vertical lines denote the median (dashed) and the mean (solid) of horizontal wind convergence derived from wind observations (CCMP).

We conclude this section with a brief discussion on ERA-Interim, which does not fall within the EC-Earth resolutions; it shows less extreme events than all three EC-Earth resolutions. This may be surprising at first sight, as data assimilation is used in ERA-Interim. An explanation should therefore probably be sought in the configurational details. ERA-Interim uses an atmospheric code based on IFS cycle Cy31r1. The IFS model underwent a change in the cloud scheme in cycle Cy25r3 (made operational on 14 January 2003), which made the atmosphere more stable, leading to less vertical motion and thus less precipitation [*Dee et al.*, 2011]. ERA-Interim uses this more stable cloud scheme, but at a resolution of only T255, thus having a combination of relatively low-resolution and the new stable cloud scheme. EC-Earth is also based on Cy31r1, but some significant changes have been included. In particular, an improved description of the entrainment of environmental air in deep convecting plumes, which was introduced in the more recent cycle 32r3, has been adopted. It greatly improved precipitation patterns over the tropics and circulation characteristics in the midlatitudes [*Hazeleger et al.*, 2012]. This new convection scheme might explain the low amount of high precipitation events in ERA-Interim compared to the EC-Earth simulations.

3.3. Wind Convergence

Strong precipitation events are tightly coupled to horizontal wind convergence and vertical velocity. Thus an analysis of the latter provides a robustness check of the precipitation results and serves to put these in a more dynamical context.

As a measure of convective activity, the distribution of vertical velocity was analyzed. As no direct measurements of vertical velocity are available, horizontal wind convergence at a height of 10 m was used as a proxy for vertical velocity. The 10 m wind fields were first regridded to the T159 grid, and then the convergence was computed with central differences. Figure 5 shows the distribution of daily mean wind convergence events at 10 m above the study area for all three EC-Earth resolutions, ERA-Interim and observations (CCMP, see data section). The distributions are positively (right) skewed with mode and median values left of the mean (see vertical lines) and a relatively long right tail. Thus even though the most frequent event is a divergence event (i.e., the median is negative), this is compensated by a wider distribution at the right-hand (convergence) side of the distribution.

The right tail with the higher values of strong wind convergence is of particular interest as they are linked to (deep) convection. This right tail of the distribution shows a clear pattern. Fully consistent with the precipitation analysis of the previous section, there is a clear increase of strong convergence events with horizontal resolution in EC-Earth. Nevertheless even T799 underestimates the strong wind convergence ($\geq 2 \cdot 10^{-5} s^{-1}$) compared to the observations. The behavior of ERA-Interim is different again. But contrary to its behavior for extreme precipitation, it shows more strong wind convergence events than all resolutions of EC-EARTH, but still less than observations. Why ERA-interim (with a resolution of T255) simulates stronger wind-convergence events than even EC-Earth T799 is unclear but we suspect it is related to the data assimilation.

3.4. Deep Convection

Czaja and Blunt [2011] showed that if certain criteria are fulfilled—namely that the moist entropy of air at the ground equals or exceeds the moist entropy at the tropopause—deep atmospheric convection can occur above oceanic boundary currents, even in winter.

To detect deep convection, it was analyzed how often vertical velocity at all pressure levels between 850 and 300 hPa (four levels in the available data) above a grid point at the ground exceeds a certain threshold. To identify slantwise convection (according to *Czaja and Blunt* occurring more often than straight upward convection), the criterion we used also allowed for going to a horizontal neighbor grid point with each new level (e.g., if the vertical velocity at the grid point directly above does not exceed the threshold, but one of its neighbors does, the criterion is fulfilled nevertheless. The check for the next level is then done from the position of this neighbor grid point). All data were analyzed on the T159 grid on 6 hourly time steps. Since the threshold is arbitrary, the analysis was repeated with several thresholds. Figure 6 shows the results for DJF with a threshold of −0.2 Pa/s.

Even though the fraction of days where the criterion is met rises with lowering the threshold, the basic pattern is always the same, with most events occurring in regions of high SSTs and high rates of occurrence over the Gulf Stream. Although we used a different diagnostic for deep convection than *Czaja and Blunt* [2011] due to the limited vertical resolution (five pressure levels) of the available model data, our results reveal a similar pattern as shown in *Czaja and Blunt* [2011]. The very high values on the coast of Greenland are caused by orographic convection and are not discussed. Figure 7 shows the mean fractions above the study region for two thresholds (–0.2 Pa/s and −0.5 Pa/s), ordered by resolution on the *x* axis. There is a clear increase in deep convection events in EC-Earth with resolution for both threshold values. We also see that with a higher threshold (–0.5 Pa/s, right plot), the sensitivity to resolution is larger than with a lower threshold (–0.2 Pa/s, left plpt). At −0.5 Pa/s, EC-Earth T799 shows 2.2 times the number events than EC-Earth T159, but at −0.2 Pa/s it just shows around 10 percent more events. The difference in number of events is however nearly the same for both thresholds. This suggests that resolution matters mostly for very strong convective events.

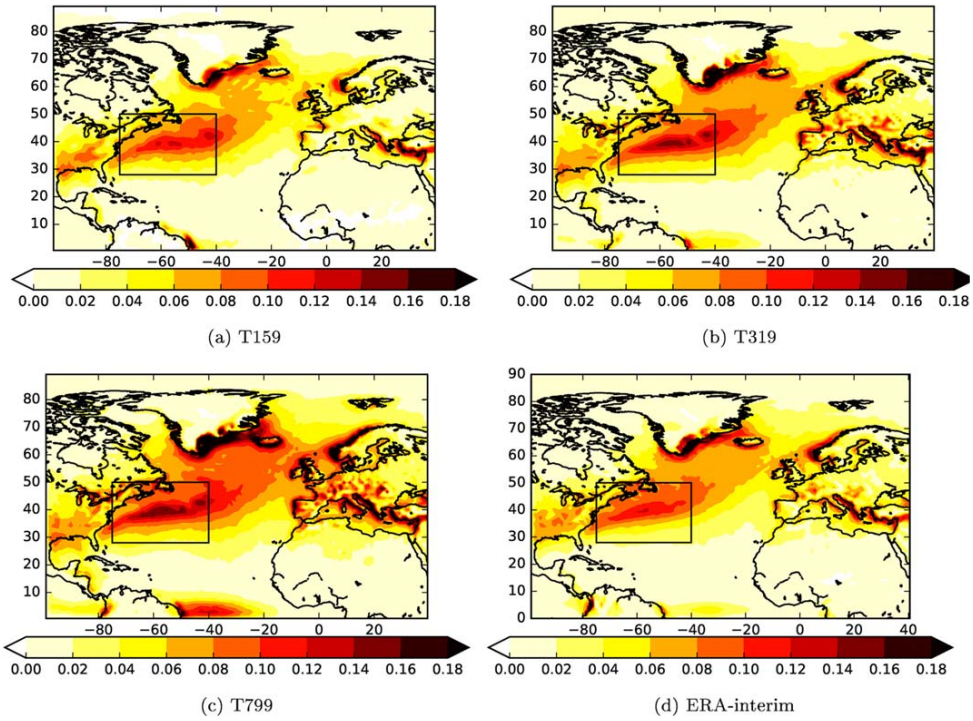

Figure 6. Fraction of wintertime deep convection events for all resolutions of EC-Earth and for ERA-interim. ($\omega < -0.2 Pa/s$ from 850 to 300 hPa, for details see text.)

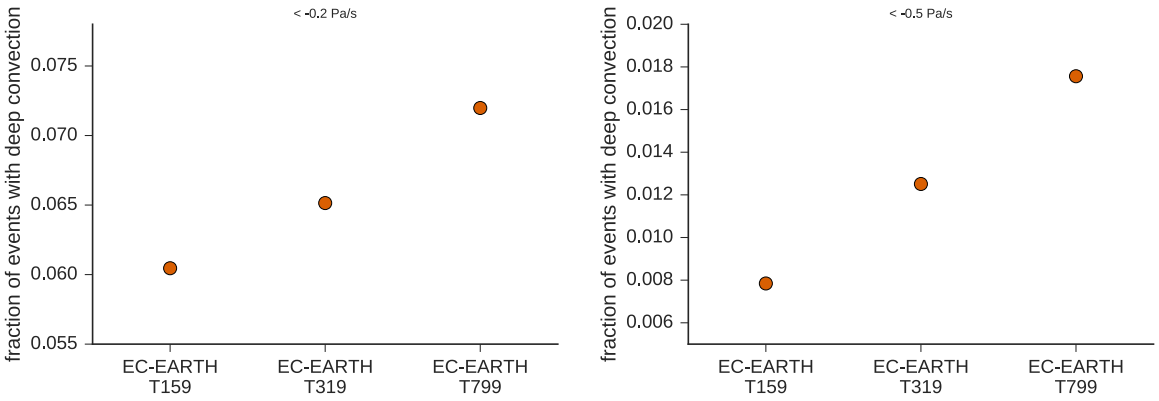

Figure 7. Fraction of wintertime events of deep convection ($\omega <$ *threshold* from 850 to 300 hPa, details see text), with threshold (left) −0.2 Pa/s and (right) −0.5 Pa/s, averaged over the study region. *x* Axis shows spectral horizontal resolution of the model. Note that the *x* axis is only categorical and not exactly scaled to horizontal resolution.

Due to the absence of direct measurements of vertical velocity and the fact that vertical velocity in reanalysis is strongly model-dependent, it cannot be judged which of the model versions and reanalyses corresponds best to reality. Nevertheless, it can be concluded that higher resolution leads to more deep convection events.

4. Summary and Conclusions

We assessed the impact of spatial model resolution on precipitation and vertical motion using an atmosphere-only GCM with three different spatial resolutions. The region of focus was the Gulf Stream region, a source region of cyclogenesis and one of the few regions outside the tropics where wintertime deep convection occurs. Our analysis showed that there is an increase in mean precipitation with resolution in most parts of this region, which is paired with more convective activity.

The impact of resolution becomes more prominent in the high-end tails of the precipitation distribution, where increasing resolution results in more intense precipitation events. This increase of the extreme events makes the high-resolution simulations agree better with the observations, though the observational record is not without ambiguities. The three observational precipitation products consulted produced different results.

The increase of extreme precipitation events is accompanied by similarly enhanced strong wind convergence and deep convection. The increased wind convergence is also beneficial as shown in a direct verification against observations. The increase in deep convection agrees with theoretical arguments put forward by *Czaja and Blunt* [2011], and together with the precipitation changes forms a consistent story.

It should also be noted that by performing atmosphere-only experiments with prescribed SSTs, ocean resolution did not put an extra constraint to resolving deep convection events, as the prescribed SST-gradients always had comparable or smaller spatial scales than the scale of air/sea interaction allowed for by the resolution of the atmospheric model. Configurations with very high atmospheric resolution, but constant ocean resolution, would not benefit from increasing atmospheric resolution as argued by *Feng et al*. [2017]. The reason is that atmospheric surface pressure adjusts to the SST-front and to optimally simulate this process the ocean resolution must resolve the relevant SST-gradient associated with the major frontal systems of western boundary currents and their midlatitude extensions, and atmospheric resolution must be compatible with these oceanic scales. A mismatch between ocean and atmospheric resolution in this respect leads to a degradation of the representation of deep convection over ocean fronts.

Acknowledgments
This paper was partly funded by the PRIMAVERA project under Grand agreement 641727 in the European Comission's Horizon 2020 research program. Era-Interim data can be obtained vie the ECMWF Web-API at ftp://apps.ecmwf.int/datasets/data/interim-full-daily. GPCP Precipitation data provided by the NOAA/OAR/ESRL PSD, Boulder, Colorado, USA, from their Web site at http://www.esrl.noaa.gov/psd/. CMORPH data obtained via Climate Explorer (https://climexp.knmi.nl/) CCMP data obtained via ftp://podaac-ftp.jpl.nasa.gov/allData/ccmp/L3.0/flk/. The EC-EARTH data used are available on the mass storage system at KNMI and can be obtained on request (haarsma@knmi.nl). TRMM data downloaded from NASA via https:/disc2.gesdisc.eosdis.nasa.gov/.

References

Adler, R. F., et al. (2003), The version-2 global precipitation climatology project (gpcp) monthly precipitation analysis (1979-present), *J. Hydrometeorol.*, *4*(6), 1147–1167.

Atlas, R., R. N. Hoffman, J. Ardizzone, S. M. Leidner, J. C. Jusem, D. K. Smith, and D. Gombos (2011), A cross-calibrated, multiplatform ocean surface wind velocity product for meteorological and oceanographic applications, *Bull. Am. Meteorol. Soc.*, *92*(2), 157–174.

Bosilovich, M. G., F. R. Robertson, and J. Chen (2011), Global energy and water budgets in MERRA, *J. Clim.*, *24*, 5721–5739.
Colle, B. A., Z. Zhang, K. A. Lombardo, E. Chang, P. Liu, and M. Zhang (2013), Historical evaluation and future prediction of eastern north American and western Atlantic extratropical cyclones in the CMIP5 models during the cool season, *J. Clim.*, *26*(18), 6882–6903.
Czaja, A., and N. Blunt (2011), A new mechanism for ocean–atmosphere coupling in midlatitudes, *Q. J. R. Meteorol. Soc.*, *137*(657), 1095–1101.
Dee, D. P., et al. (2011), The era-interim reanalysis: Configuration and performance of the data assimilation system, *Q. J. R. Meteorol. Soc.*, *137*(656), 553–597, doi:10.1002/qj.828.
Feng, X., B. Huang, B. P. Kirtman, J. L. Kinter III, and L. S. Chiu (2017), A multimodel analysis of the resolution influence on precipitation climatology in the Gulf Stream region, *Clim. Dyn.*, *48*, 1685–1704.
Flato, G., et al. (2013), Evaluation of climate models, in *Climate Change 2013: The Physical Science Basis. Contribution of Working Group I to the Fifth Assessment Report of the Intergovernmental Panel on Climate Change*, edited by T. F. Stocker, pp. 741–866, Cambridge Univ. Press, Cambridge, U. K.
Haarsma, R. J., W. Hazeleger, C. Severijns, H. de Vries, A. Sterl, R. Bintanja, G. J. van Oldenborgh, and H. W. van den Brink (2013), More hurricanes to hit western Europe due to global warming, *Geophys. Res. Lett.*, *40*, 1783–1788, doi:10.1002/grl.50360.
Hazeleger, W., et al. (2012), EC-earth v2. 2: Description and validation of a new seamless earth system prediction model, *Clim. Dyn.*, *39*(11), 2611–2629.
Huffman, G. J., R. F. Adler, M. M. Morrissey, D. T. Bolvin, S. Curtis, R. Joyce, B. McGavock, and J. Susskind (2001), Global precipitation at one-degree daily resolution from multisatellite observations, *J. Hydrometeorol.*, *2*(1), 36–50.
Huffman, G. J., R. F. Adler, D. T. Bolvin, and E. J. Nelkin (2010), The TRMM multisatellite precipitation analysis (TMPA), in *Satellite Rainfall Applications for Surface Hydrology*, edited by F. Hoissain and M. Gebremichael, pp. 3–22, Springer, Dordrecht, Netherlands.
Jones, P. W. (1999), First-and second-order conservative remapping schemes for grids in spherical coordinates, *Mon. Weather Rev.*, *127*(9), 2204–2210.
Joyce, R. J., J. E. Janowiak, P. A. Arkin, and P. Xie (2004), Cmorph: A method that produces global precipitation estimates from passive microwave and infrared data at high spatial and temporal resolution, *J. Hydrometeorol.*, *5*(3), 487–503.
Jung, T., et al. (2012), High-resolution global climate simulations with the ECMWF model in Project Athena: Experimental design, model climate, and seasonal forecast skill, *J. Clim.*, *25*(9), 3155–3172.
Kitoh, A., and H. Endo (2016), Changes in precipitation extremes projected by a 20-km mesh global atmospheric model, *Weather Clim. Extrem.*, *11*, 41–52.
Ma, X., P. Chang, R. Saravanan, R. Montuoro, J.-S. Hsieh, D. Wu, X. Lin, L. Wu, and Z. Jing (2015), Distant influence of Kuroshio eddies on north pacific weather patterns?, *Nat. Sci. Rep.*, *5*, 17785, doi:10.1038/srep17785.
Minobe, S., A. Kuwano-Yoshida, N. Komori, S.-P. Xie, and R. J. Small (2008), Influence of the Gulf Stream on the troposphere, *Nature*, *452*(7184), 206–209.
Reynolds, R. W., T. M. Smith, C. Liu, D. B. Chelton, K. S. Casey, and M. G. Schlax (2007), Daily high-resolution-blended analyses for sea surface temperature, *J. Clim.*, *20*(22), 5473–5496.
Small, R. J., R. A. Tomas, and F. O. Bryan (2014), Storm track response to ocean fronts in a global high-resolution climate model, *Clim. Dyn.*, *43*(3–4), 805–828.
Stephens, G. L., T. L'Ecuyer, R. Forbes, A. Gettelmen, J.-C. Golaz, A. Bodas-Salcedo, K. Suzuki, P. Gabriel, and J. Haynes (2010), Dreary state of precipitation in global models, *J. Geophys. Res.*, *115*, D24211, doi:10.1029/2010JD014532.
van der Wiel, K., S. B. Kapnick, G. A. Vecchi, W. F. Cooke, T. L. Delworth, L. Jia, H. Murakami, S. Underwood, and F. Zeng (2016), The resolution dependence of contiguous US precipitation extremes in response to CO2 forcing, *J. Clim.*, *29*(22), 7991–8012.
van Haren, R., R. J. Haarsma, G. J. van Oldenborgh, and W. Hazeleger (2015), Resolution dependence of European precipitation in a state-of-the-art atmospheric general circulation model, *J. Clim.*, *28*, 5134–5149, doi:10.1175/JCLI-D-14-00279.1.
Yang, Q., L. R. Leung, S. A. Rauscher, T. D. Ringler, and M. A. Taylor (2014) Atmospheric moisture budget and spatial resolution dependence of precipitation extremes in aqua planet simulations, *J. Clim.*, *27*, 3565–3581.
Zappa, G., L. C. Shaffrey, and K. I. Hodges (2013), The ability of cmip5 models to simulate north Atlantic extratropical cyclones, *J. Clim.*, *26*(15), 5379–5396.